NEURAL NETWORK BASED OPTIMIZATION OF AN IPMSM WITHIN A BLDC DRIVE

Mitja Garmut, Simon Steentjes*, Martin Petrun

University of Maribor, FERI, Institute of Power Engineering
Koroška cesta 46, SI-2000 Maribor, Slovenia, e-mail: mitja.garmut@um.si, martin.petrun@um.si

*Hilti Entwicklungsgesellschaft mbH
Hiltistraße 6, DE-86916 Kaufering, Germany, e-mail: simon.steentjes@hilti.com

***Abstract* - This paper introduces a neural network based optimization framework for Interior Permanent Magnet Synchronous Machines (IPMSMs) in squarewave drive applications (i.e., Brushless Direct Current or BLDC drives) for enhanced machine performance. The focus was on reducing torque ripple while enhancing or maintaining the torque-to-current ratio. A Finite Element Method model and a Design of Experiments are employed to generate training data for neural networks. The networks enabled a multi-objective optimization, producing two designs that significantly reduce torque ripple and simultaneously increase average torque. A significant decrease in simulation time alongside an innovative approach to designing IPMSMs for squarewave drives is presented.**

I. INTRODUCTION

Interior Permanent Magnet Synchronous Machines (IPMSM) are often driven by a two-level three-phase voltage source inverter by applying a squarewave (i.e., 120° commutation, block or six-step) control. Such a system is commonly referred to as a Brushless Direct Current (BLDC) drive. Operating these systems requires measuring direct current (DC) and merely six position states, provided by three Hall sensors, resulting in simplicity and cost-effectiveness. In recent years, the research on this topic has picked up [1, 2]. A common problem when operating with squarewave control is high torque ripple. To enhance the drive's performance, the primary objective was to minimize torque ripple without compromising the torque-to-current ratio. We analyzed the impact of torque ripple reduction on the torque-to-current ratio. First, a parametric Finite Element Method (FEM) model of the IPMSM was constructed, which was used to perform a simulation exited by an ideal-shaped squarewave current. A Design of Experiment (DoE) approach was used to collect simulation results to train a feedforward Neural Network (NN) [3]. A multi-objective optimization was performed to evaluate how the minimal torque ripple is connected to the torque-to-current ratio. Two designs were selected for detailed analysis.

II. THEORETICAL BACKGROUND

A. abc model of an IPMSM

The voltage-balance equation of the IPMSM in the abc reference frame is given by (1)

$$\mathbf{u}_{\mathrm{abc}} = \mathbf{R}\mathbf{i}_{\mathrm{abc}} + \frac{\mathrm{d}}{\mathrm{d}t}[\mathbf{L}(\theta)\mathbf{i}_{\mathrm{abc}} + \boldsymbol{\Psi}_{\mathrm{m}}(\theta)], \qquad (1)$$

where $\mathbf{i}_{\mathrm{abc}} = [i_{\mathrm{a}}\ i_{\mathrm{b}}\ i_{\mathrm{c}}]^{\mathrm{T}}$ are the phase currents, $\mathbf{u}_{\mathrm{abc}} = [u_{\mathrm{a}}\ u_{\mathrm{b}}\ u_{\mathrm{c}}]^{\mathrm{T}}$ are the phase voltages, $\boldsymbol{\Psi}_{\mathrm{m}}(\theta) = [\Psi_{\mathrm{ma}}\ \Psi_{\mathrm{mb}}\ \Psi_{\mathrm{mc}}]^{\mathrm{T}}$ are the permanent magnet flux linkages, $\mathbf{R} = diag(R\ R\ R)$ are the phase resistances of the stator windings, $\mathbf{L}(\theta)$ is the inductance matrix and θ is the electrical angle. The electromagnetic torque is defined as (2)

$$t_{\mathrm{e}} = p_{\mathrm{p}}[\mathbf{i}_{\mathrm{abc}}^{\mathrm{T}}\frac{\partial\boldsymbol{\Psi}_{\mathrm{m}}(\theta)}{\partial\theta} + \frac{1}{2}\mathbf{i}_{\mathrm{abc}}^{\mathrm{T}}\frac{\partial\mathbf{L}(\theta)}{\partial\theta}\mathbf{i}_{\mathrm{abc}}], \qquad (2)$$

where p_{p} is the number of pole pairs.

Squarewave-shaped phase currents $\mathbf{i}_{\mathrm{abc}}$, shown in Fig. 1b) were used to excite the delta-connected 6-slot 4-pole IPMSM with Nd-Fe-B magnet and a fractional slot non-overlapping winding. In Fig. 1 the ideal squarewave-shaped current of a delta connected machine and the back Electro Motive Force (EMF) $\mathbf{e}_{\mathrm{abc}}$ are presented, where I_{p} is he peak current value and e_{p} is the peak EMF value. The advance commutation angle α was defined as the phase shift between the fundamental harmonic component of i_{b} and e_{b} and was in this analysis set to zero.

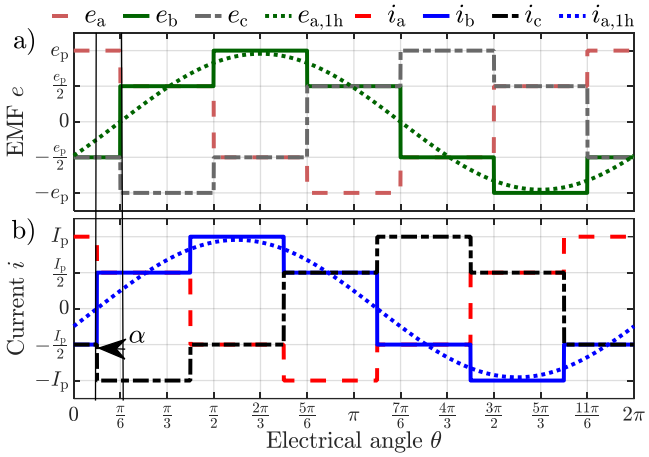

Figure 1: a) ideal shape of back EMF, b) ideal squarewave-shaped current of a delta-connected machine and advance commutation angle definition.

B. Optimisation of an IPMSM rotor

First, a parametric FEM model of the IPMSM in ANSYS Maxwell 2D was set up where 5 parameters were optimized, 1 on the stator (θ_{v} - slot opening angle), and 4 on the rotor (d_{rd}, d_{rq}, d_{ry} and θ_{m}), which are shown in Fig. 2.

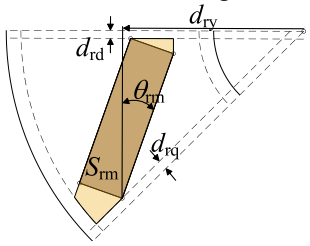

Figure 2: Parametric geometry of IPMSM

The magnet area S_{rm} was assumed constant. The input in the FEM simulation was the $\mathbf{i}_{abc}$ and the output were the torque ripple $t_{e,ripp}$ and the average torque $t_{e,avg}$. All presented parameters were scaled to the inner radius of the stator.

An automated DoE (applying latin hypercube sampling) was performed using 6000 samples. In the next step, two feedforward NN were trained, where 5 inputs (i.e., design parameters) and 1 output (i.e., te,ripp and te,avg) were used. The Levenberg-Marquardt training function was employed and three hidden layers (20, 60, 20) were used. Fig. 3 shows the regression plot of the trained NN for both datasets.

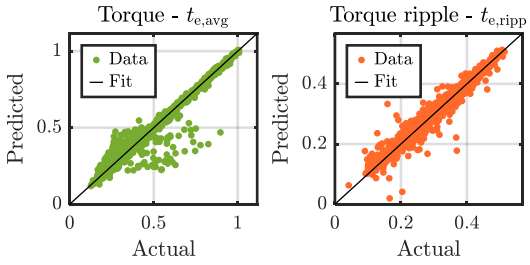

Figure 3: Regression plot of the trained NN

A two-objective optimization was performed using a multi-objective genetic algorithm in Matlab. The two objectives were minimizing $t_{e,ripp}$ and maximizing $t_{e,avg}$. The Pareto front with the 2 selected designs and reference design are shown in Fig. 4.

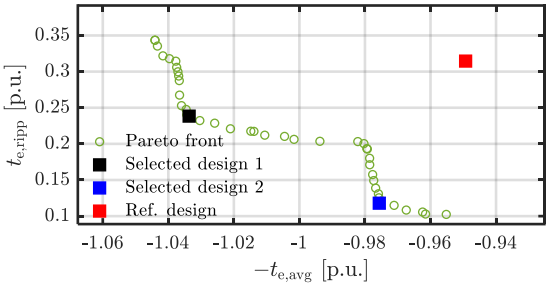

Figure 4: Pareto front with the selected designs

The selected design 1 was chosen in a way that the $t_{e,avg}$ was maximized, but $t_{e,ripp}$ was stil reduced. The selected design 2 was chosen in a way that $t_{e,avg}$ was still improved and the $t_{e,ripp}$ was reduced significantly. The design parameters are shown in Table I.

III. RESULTS

The two designs were reevaluated within FEM simulations to exclude the inherent error margin of the NN.

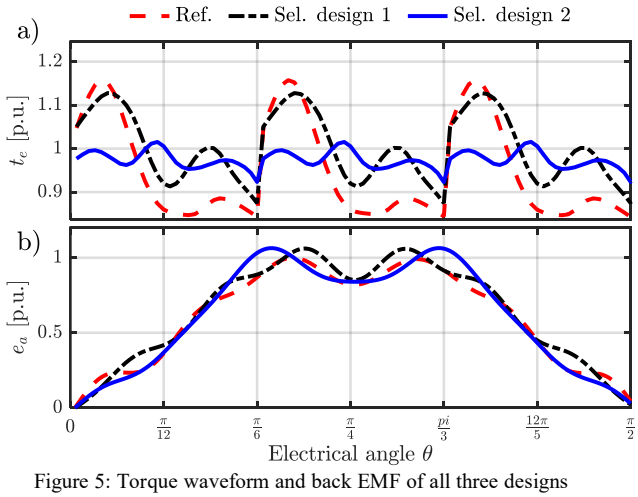

Figure 5: Torque waveform and back EMF of all three designs

Fig. 5 presents the back EMFs and the electromagnetic torque t_e of the selected designs and reference design and Table I presents the optimized values of the discussed machine designs.

TABLE I
OPTIMIZATION AND DESIGN VALUES

	Ref. design	Design 1	Rel. to ref.	Design 2	Rel. to ref.
$t_{e,ripp}$ [p.u.] – NN	/	0.238	/	0.1179	/
$t_{e,ripp}$ [p.u.] – FEM	0.3146	0.2531	-19.6%	0.0925	-70.6%
$t_{e,avg}$ [p.u.] – NN	/	1.033	/	0.975	/
$t_{e,avg}$ [p.u.] – FEM	0.949	1.003	5.7%	0.974	2.6%
d_{rd} [p.u.]	0.074	0.001	/	0.002	/
d_{rq} [p.u.]	0	0.13	/	0.037	/
d_{ry} [p.u.]	0.563	0.675	/	0.733	/
θ_m [°]	0	-24.90	/	18.7	/
θ_m [°]	7.5	6.7	/	7.8	/

Design 1 showed 19.6% reduction of the $t_{e,ripp}$ and 5.7% increase of the $t_{e,avg}$ compared to the reference design after the FEM analysis. The waveform of the t_e did not change significantly in contrast to the reference design. The increase in $\mathbf{e}_{abc}$ led to a higher $t_{e,avg}$, further amplified by the decreased value of the $t_{e,ripp}$. The rotor in design 1 featured a V-shaped magnet configuration.

Design 2 reduced the $t_{e,ripp}$ significantly by 70.6% and increased the $t_{e,avg}$ by 2.6% compared with the reference design. The shape of $\mathbf{e}_{abc}$ aligned better with $\mathbf{i}_{abc}$, causing $t_{e,ripp}$ reduction and still increasing $t_{e,avg}$. In design 2, the rotor's configuration positioned the magnets along the outer perimeter.

IV. CONCLUSIONS

A successful implementation of NN in two-objective machine optimization was showcased. By employing NN as meta-models of respective FEM models within the optimization workflow, the simulation time was reduced by a factor of 5. This workflow enabled the saving of all machine data during the DoE step, allowing for various types of optimization in post-processing using NN.

Both optimized designs show a reduction of $t_{e,ripp}$ and an increase of $t_{e,avg}$, with a minor trade-off in the secondary objective. The initial goal was achieved by reducing the $t_{e,ripp}$ and additionally improving the torque-to-current ratio with both designs. Design 1 featured a V-shape and design 2 pushed the magnets to the outer perimeter.

As the current waveform for optimization was idealized as a squarewave, the gained effect will be checked at a system-level simulation in the full paper. There the current waveform $\mathbf{i}_{abc}$ and the α change because of the commutation interval, which is a consequence of activating individual windings and their leakage inductance.

REFERENCES

[1] J. Zhou, J. Lu, S. Ebrahimi, and J. Jatskevich, "A Compensation of Commutation Angle in Hall-Sensor-Controlled Brushless DC Motors for Maximum Torque per Ampere Operation," in *2022 21st International Symposium INFOTEH-JAHORINA (INFOTEH)*, 2022-03-16 2022: IEEE, doi: 10.1109/infoteh53737.2022.9751320.

[2] D. Mohanraj *et al.*, "A Review of BLDC Motor: State of Art, Advanced Control Techniques, and Applications," *Ieee Access,* vol. 10, pp. 54833-54869, 2022-01-01 2022, doi: 10.1109/access.2022.3175011.

[3] V. Parekh, D. Flore, and S. Schops, "Variational Autoencoder-Based Metamodeling for Multi-Objective Topology Optimization of Electrical Machines," *IEEE Transactions on Magnetics,* vol. 58, no. 9, pp. 1-4, 2022-09-01 2022, doi: 10.1109/tmag.2022.3163972.